Published in final edited form as:
Proc SPIE Int Soc Opt Eng. 2018 February ; 10578: . doi:10.1117/12.2292564.

Use of material decomposition in the context of neurovascular intervention using standard flat panel and a high-resolution CMOS detector

A.R. Podgorsak[a,b], **A.C. Venkataraman**[b], **S.V. Setlur Nagesh**[b], **D.R. Bednarek**[b,c], **S. Rudin**[a,b,c,d], **A. Siddiqui**[b,d], and **C.N. Ionita**[a,b]

[a]Department of Biomedical Engineering, University at Buffalo

[b]Toshiba (Canon) Stroke and Vascular Research Center, Buffalo, NY

[c]Department of Radiology, University at Buffalo

[d]Department of Neurosurgery, University at Buffalo

Abstract

The imaging of endovascular devices during neurovascular procedures such as the coiling of aneurysms guided with CBCT imaging may be challenging due to the presence of highly attenuating materials such as platinum in the coil and stent marker, nickel-titanium in the stent, iodine in the contrast agent, and tantalum in the embolization agent. The use of dual-energy imaging followed by a basis material decomposition image processing-scheme may improve the feature separation and recognition. Two sets of testing were performed to validate this concept. The first trial was the acquisition of dual-energy micro-CBCT data of a 3D-printed simple aneurysm model using a 49.5 μm pixel size CMOS detector (Teledyne DALSA, Waterloo, ON.). Two sets of projection data were acquired using beam energies of 35 kVp and 70 kVp. Axial slices were reconstructed and used to carry out the material decomposition processing. The second trial was the acquisition of dual-energy CBCT images of a RS-240T angiographic head phantom (Radiology Support Devices Inc., CA.) with an iodine vascular insert using a Toshiba Infinix BiPlane C-arm system coupled to a flat panel detector. Two sets of image data were acquired using beam energies of 80 kVp and 120 kVp. Following image reconstruction, slices of the phantom were decomposed using the same processing as previously. The resulting image data over both trials indicate that the decomposition process was successful in separating the kinds of materials commonly used during a neurovascular intervention, such as platinum, cobalt-chromium, and iodine. The normalized root mean square error metric was used to quantitatively assess this. This indicates a basis for future more clinically relevant testing of our methods.

Keywords

Material decomposition; micro-CT; dual-energy CT; image-guided neurosurgery

1. INTRODUCTION

Spectroscopy methods for material analysis have led to greater understanding of material identification and behavior[1]. The implementation of these advances into medical imaging has been delayed by detector and x-ray source limitations. Until recently, single-spectrum CT scanners have been the gold standard for patient image acquisition due to its ability for 3D visualization of internal structures. However, this approach is not optimal due to measurement errors related to the inability to differentiate x-ray photons with different energies. Recent advances in detector technologies, rapid kVp switching, and software can allow for the translation of such spectroscopic methods to clinical medical imaging. There is a need for such methods in the endovascular operating room, where image-guided minimally invasive procedures are quickly becoming the preferred technique for treating conditions such as an aneurysm, stenosis, or arteriovenous malformations (AVM).

In regions of complex anatomy such as the brain, correct diagnosis of various medical conditions can be impaired due to the inability to differentiate between materials that show up similarly when imaged using a single spectrum CBCT scan. Such an occurrence can be due to the placement of a stent or platinum coil in the brain vasculature in order to treat an aneurysm. The high Z stent and coil may lie close in proximity to each other, as well as to any iodine contrast agents that may be included in the space to aid in the imaging. All of these similarly attenuating materials may have little contrast when visualized with a single-spectrum CBCT scan, and all of these high Z materials can lead to imaging artifacts such as beam hardening, which further inhibit the usefulness of the images acquired[2]. It is for these reasons that neurovascular interventionists have great need for spectral CT used during image-guided neuro-interventions. The errors present during single spectrum imaging could be solvable using multi-spectral CT methods such as dual-energy CT. The use of dual-energy CBCT leads to the acquisition of information regarding how the attenuation of the different materials depends on energy, allowing for a more complete separation of materials present in a scanned anatomical region[3]. Material decomposition is able to utilize this dual-energy scan data to obtain more information regarding the imaged object than single-energy CT could attain.

Material decomposition is a method that relies on the variation of a material's attenuation coefficient as the incident x-ray beam energy changes. Figure 1 contains a plot that shows how the attenuation coefficient of four commonly used materials in neurovascular intervention changes as the x-ray beam energy varies in the diagnostic energy range. Generally, as the beam energy increases, the attenuation coefficient decreases. This generality breaks down at the material's absorption edges. Due to the large spike in attenuation coefficient, this energy can be considered to attempt to separate similarly attenuating materials during dual-energy imaging.

The general concept of a dual-energy CT scan coupled with material decomposition involves the acquisition of two datasets of the scanned objects, one using a low beam energy and one using a higher energy x-ray beam[5]. As shown in Fig. 1, the attenuation coefficients of the materials that make up the object will vary between the two acquisition energies. Materials are separated by how their level of x-ray attenuation changes between the energies used for the two acquisitions. Material decomposition is capable of showing the contribution of each of the materials to each reconstructed voxel in the reconstructed image space. In this way, visualization of specific portions of complex anatomy may be improved.

In the literature, there are many implementations of material decomposition using different types of CT image acquisition techniques[6, 7], and using image data of different types of the body[8, 9]. We looked to explore this concept of using dual-energy CBCT in a basis material decomposition image-processing scheme specifically to solve the difficulty in imaging the neurovascular anatomy following an endovascular procedure such as the deployment of a stent or coil. We additionally wanted to investigate any potential detector dependencies that the material decomposition method may possess.

Generally, material decomposition makes some assumptions regarding the anatomy of the scanned object. We assume that every unknown material can be mathematically represented as fractions of other, simpler materials. This makeup in this context is related to how the attenuation coefficient of the different materials varies over the range of acquisition energies used.

In order to solve some of the challenges present in image-guided procedures in the neurovascular space, we performed a study to determine how material decomposition might improve the image guidance of procedures such as the stenting and coiling of cerebral aneurysms, or the embolization of AVMs.

2. MATERIALS AND METHODS

The specific method we employed to perform the material decomposition is based off a method introduced in a paper[10] by Friedman and colleagues. This method requires a further assumption to be made regarding the scanned object. Firstly, the claim is made that the object can be represented by no more than three materials we will denote as basis materials from here on out. This means that every unknown material X can be represented by the summation of some percentage of each of the three basis materials. We can then define our system using three equations, and possessing three unknowns (the percentage each basis material makes up the unknown material), making it a solvable system. The system can be found in Equation 1.

$$
\begin{aligned}
&\mu_{1,\,LokVp} \times c_1 + \mu_{2,\,LokVp} \times c_2 + \mu_{3,\,LokVp} \times c_3 = \mu_{X,\,LokVp} \\
&\mu_{1,\,HikVp} \times c_1 + \mu_{2,\,HikVp} \times c_2 \mu_{3,\,HikVp} \times c_3 = \mu_{X,\,HikVp} \\
&c_1 + c_2 + c_3 = 1
\end{aligned}
\quad (1)
$$

where $\mu_{X.LokVp}$ is the considered voxel's value in the acquired slice at the low beam energy. $\mu_{X.HikVp}$ is the considered voxel's value in the acquired slice at the high beam energy. $\mu_{1,2,3|LokVp}$ is the voxel value of a pure amount of the basis material considered at the low beam energy. $\mu_{1,2,3|HikVp}$ is the voxel value of a pure amount of the basis material considered at the high beam energy. $c_{1,2,3}$ are the fractions each basis material makes up the considered voxel. Each voxel has its intensity input into the system as μ_x at either low or high kVp. $\mu_{1,\,2,3|Lo,HikVp}$ is the voxel value at either low or high kVp of a calibration amount of one of the basis materials. A pure sample of each of the three basis materials must have been imaged at the acquisition energies prior to the decomposition for use in calibrating the system. This system is solved using all of the reconstructed voxels, so that each voxel's fractional makeup via the basis materials has been computed. Using this information, each reconstructed slice is re-displayed using a linear mapping of the c_1 c_2 and c_3 term. The calibration sample and any other pure region of the basis material will be displayed as maximum intensity. This intensity will decrease as less of the basis material is present in the considered voxel, going all the way to zero when the voxel is devoid of the basis material. In this way, a slice of image data filled with unknown materials can be redisplayed as percentages of known materials, potentially giving clinicians viewing the images more information regarding the anatomical region in question. Following this decomposition process, resultant slices are passed through a threshold to reduce the impact of spurious signal, and then assigned to a color channel. The entire reconstructed volume can then be viewed where each basis material is differentiated by a different color, indicating their makeup based on the three basis materials and the percentages that make up the object being imaged.

Two trials were proposed to study the feasibility of this decomposition process on images acquired of the neurovascular space. Firstly, a patient specific simple aneurysm model was 3D-printed and two endovascular interventions were carried out using it. We simulated a stent assisted coiling aneurysm treatment. A platinum coil was deployed into the aneurysm dome, and a stent was placed across the aneurysm orifice to prevent the coil from expanding into the main vessels. Iodine contrast agent was added to the model to simulate a condition where a thrombosed aneurysm is being imaged. In such as case, the iodine would not be expected to enter the aneurysm orifice. A projection image of the model prior to the addition of the contrast agent can be found in Figure 2. Image data acquisition of this phantom was performed with our in-house developed micro-CT system[11] coupled to a 49.5 μm CMOS detector made by Teledyne DALSA. As this is a dual-energy method, two consecutive scans of the object were performed, with care taken not to move the object at all between the two to ensure good registration. Data was acquired both prior to and following the addition of the iodine contrast agent. Image acquisition of the aneurysm model was performed using tube voltages of 35 kVp and 70 kVp. These parameters were selected to attempt to maximize the variation in attenuation coefficient between the two energies, thus ensuring the best possible chance for an effective decomposition. All other tube and image acquisition parameters were kept constant across the two scans, notable ones being a tube power of 50 W, integration time of 1 second per frame, and 0.5 mm of aluminum for beam filtration. Following the acquisition of the dual-energy image data, volume reconstruction was performed for each set using a standard FDK algorithm[12] modified with a self-centering computation[13] prior to backprojection. Reconstruction parameters were kept identical between the two acquisitions, notably a 35 μm voxel size. The reconstructed data is input into the decomposition process.

The second trial was carried out using the RS-240T angiographic head phantom (Figure 3) made by Radiology Support Devices Inc. as the scanned object. This phantom has a 3-Dimensional high contrast vascular pattern using iodine on one side of the head, as well as a full bone skull surrounding a plastic material to simulate the soft tissue of the brain. This makes it an ideal object to perform a more clinically relevant testing of the material decomposition method. Image acquisition of this phantom was carried out using a Toshiba Infinix-i Biplane C-arm system, coupled to a standard flat panel detector system. Beam energy for this trial was 80 and 120 kVp, which matches what would be selected in clinical dual-energy CT image acquisitions. Similar to the first trial, axial slices of the head phantom were reconstructed to be used in the decomposition process.

As output from the decomposition process, decomposed slices of image data are obtained. In order to quantify the performance of the decomposition process and to make it easier to tune the algorithm for better decompositions, there needs to be a method for the quantitative assessment of the decompositions. The method that was selected is the Normalized Root Mean Square Error (NRMSE) metric[14]. The NRMSE metric measures differences between expected and observed values of a system, normalized by the intensity of the measurements. This metric is defined in Equation 2.

$$\%\,\mathrm{NRMSE} = \frac{100}{f_{\max}^{\mathrm{meas}} - f_{\min}^{\mathrm{meas}}}\sqrt{\sum_{j=1}^{v}\frac{\left(f_j^{\mathrm{ref}} - f_j^{\mathrm{meas}}\right)^2}{v}} \qquad (2)$$

%NRMSE is the percent normalized root mean square error metric. The summation of the interior terms is performed on every voxel in the redisplayed slice. $f_{\max}^{\mathrm{meas}}$ is the maximum value in the slice. $f_{\min}^{\mathrm{meas}}$ is the minimum value in the slice. f_j^{ref} is the expected value of the considered voxel. f_j^{meas} is the measured value of the considered voxel. v is the number of voxels present in the slice. We restrict the computation of %NRMSE to voxels For this type of quantitative assessment, there is prior knowledge of the object that is imaged and decomposed, thus limiting its use to phantoms. In a clinical situation, a different metric will have to be developed. The prior knowledge of the phantom allows us to input f_j^{ref} into Equation 2, comparing what the decomposition is telling regarding the material makeup of the scanned object with the object's "true" material makeup. An accurate decomposition is one that shows agreement with prior knowledge of the scanned object, thus will have a small value for %NRMSE. A single slice of image data is empirically used for this calibration step. The same slice is used for all of the comparisons between decompositions. The rest of the slices are used for the %NRMSE computation.

Going into the image acquisition portion of this work, we anticipated that we would be able to perform a decomposition using both of the scanned objects using our algorithm. Previous work[15] carried out by our group has suggested that as long as the basis materials selected are high Z, the decomposition should be able to be carried out with high accuracy, and a low computed %NRMSE below 10%.

3. RESULTS

Projection data as well as a selected reconstructed slice for the high-energy acquisition of the simple aneurysm model prior to the inclusion of the iodine contrast agent can be found in Figure 4. Visible in both the projection and the slice are the cobalt-chromium stent as well as the platinum coil. The decomposition result using the slice in Fig. 4b as well as the low-energy equivialent can be found in Figure 5. The basis materials derived for this acquisiton were the cobalt-chromium (Fig. 5a) and the platinum (Fig. 5b). Included in the figure is the basis mapping for both the cobalt-chromium and the platinum, as well as the two slices re-colored and overlaid onto each other and displayed together (Fig. 5c). In this case, red represents the platinum and green represents the cobalt-chromium. Additionally included in image 5a is a blue arrow indicating a reigon of error present in the decomposed map of the cobalt-chromium.

Projection data as well as a selected reconstructed slice for the simple aneurysm model following the inclusion of the iodine can be found in Figure 6. The projection selected is following a 180° rotation from the orientation of the phantom in Fig. 4. Visible in the images are the iodine contrast agent, the cobalt-chromium stent, and the platinum coil. The decomposition result using the slice in Fig. 6b as well as its low energy equivalent can be found in Figure 7. The basis materials derived for this acquisiton were the cobalt-chromium, the platinum, as well as the iodine. Included in the figure is the basis mapping for the platinum (Fig. 7a), cobalt-chromium (Fig. 7b), and iodine (Fig. 7c), as well as the three slices re-colored and overlaid onto each other and displayed together. In this case, red represents the platinum, blue represents the cobalt-chromium, and green represents the iodine. Additionally included in image 7b is a blue arrow indicating a region of error in the decomposed map of the cobalt-chromium.

An example of a reconstructed slice of the RS-240T angiographic head phantom can be found in Figure 8a. This slice was computed using the high energy scan data. Visible in the slice is the vascular insert, as well as the outer skull region of the phantom. The result of the decomposition using that slice and its low energy equivalent comprises the rest of Figure 8, where 8b is the iodine mapping, and 8c is the bone mapping. The two decomposed slices were then recolored and overlaid onto each other, then displayed in Fig. 8d. Here, green represents the bone and red represents the iodine. A maximum intensity projection of the volumetric rendering of all of the recolored slices in the stack can be found in Figure 9.

4. DISCUSSION

The goal of this work was to perform some initial testing of the use of material decomposition on images of neurovasculature. Our initial findings suggest that the image-guidance used during endovascular procedures such as the stent and coil embolization of aneurysms may be improved using dual-spectrum CT coupled to material decomposition, dependent on the results of further testing.

The projection data shown in Fig. 4a can be thought of as a best-case scenario in the context of imaging the neurovascular anatomy following the deployment of devices into and around the aneurysm sac. There is no contrast present, and there is some spatial separation between the two materials in the majority of the planes of the object data. However, there are some planes where the two materials are close. Additionally degrading the image quality in these regions is the presence of image artifacts in-between the struts of the stent due to a hardening of the x-ray beam as it passes through the stent. The artifacts display materials with incorrect image intensity, thus complicating decomposition methods that use image intensity to separate out materials. In this case, the decomposition was carried out using just two basis materials, providing good separation of the basis materials in almost all of the voxels.

Qualitatively, the platinum map is completely devoid of signal in all regions except where the platinum marker was. The cobalt-chromium was properly discriminated from in all of the struts, except for one region in the cobalt-chromium map (blue arrow Fig. 5a) where there is error present. This appears to be limited to the edge of the platinum marker having reduced image intensity due to partial volume averaging, and being decomposed as cobalt-chromium instead of the platinum. The rest of the platinum is properly displayed as platinum, so no intensity in the cobalt-chromium map and maximum intensity in the platinum map. Interestingly, the streaks which were present between the struts in the input reconstructed slice were not displayed as either of the two materials. This makes some sense, as their image intensity is much lower than that of either of the two basis materials. What is also apparent regarding the cobalt-chromium is the shape of the decomposed struts. It does not appear that the decomposition has properly maintained the shape of the struts from reconstruction. When the two mappings are recolored and overlaid onto each other (Fig. 5c), a better picture of the original scan data begins to form.

The computation of the %NRMSE (Table 1) was below 10% for both of the basis materials, the cobalt-chromium and the platinum. The cobalt-chromium error was computed to be higher than the platinum error, matching what would be expected due to the region of error in the cobalt-chromium mapping. Additionally, the shape of the struts seems to have been negatively impacted by the artifacts present in the image, as they do not seem to match up with what would be the expected shape of a stent strut. This error can mostly be attributed to the image artifacts present in the image data, such as partial volume averaging.

The projection data shown in Fig. 6a is a more clinically relevant case, following the addition of the iodine contrast agent to the simple aneurysm model. In this case, there will be slices of image data where all three of the materials will be present and in close proximity to one another. The addition of the iodine also increases the potential for reconstruction artifacts to be present in the area, as there are more highly attenuating materials in the vicinity of the anatomy in question.

When the decomposed maps are considered, there appears to be good separation between the three materials. Similar to the previous decomposition, there is an error present in the cobalt-chromium map at the location corresponding to the edge of the platinum marker. This is likely due to the same reason as during the previous decomposition, that being partial volume averaging at the edges of the marker. This changes the voxel intensity enough for the decomposition process to display the voxels as being cobalt-chromium instead of the platinum. Additionally, the struts of the cobalt chromium stent were not decomposed to retain the proper shape of the struts. This will lead to an increase in the computed error of that map. The iodine and platinum maps appear to be decomposed properly, and were expected to have lower amplitude computed error. Following the recoloring and overlaying of the three materials, a more complete picture of the selected slice begins to form.

The computation of %NRMSE (Table 2) matched our expectation at the onset of the work. The iodine and platinum maps were computed accurately, and they had the lower computed error. The cobalt-chromium had regions of error present in the image data, leading to a higher computed error. Even so, the error was computed to be below the 10% threshold that was set at the onset of this work. It is notable that the addition of the iodine caused the computed error of both the platinum and the cobalt-chromium to increase when compared with the levels prior to the addition of the iodine. This matches our expectation, as there are more artifacts present in the image data to affect the reconstructed voxel intensity, thus influencing the accuracy of the decomposition.

The case of the RS-240T angiographic head phantom is a further step towards clinically relevant examples. The selected reconstructed slice shown in Fig. 8a shows how similarly the iodine and bone may be displayed as in a reconstructed slice depending on the concentration of the iodine. Present in the selected slice were similar artifacts to the previous two examples, notably a degradation of the accuracy of the shape of the iodine insert in the phantom. In this case, a misalignment of the rotational axis of the object and the imaging system may have been to blame for this. When the result of the decomposition is qualitatively assessed, there appears to be good agreement between the material maps and true object data, as confirmed by the recoloring and overlaying of the maps. The maximum intensity projection in Fig. 9 shows a different way that this method could redisplay the image data, depending on how the clinician wishes to view it. The decomposition process was deemed able to utilize the anatomical information collected from a flat panel detector, based on the results of this decomposition.

An important limitation to this described method is the use of basis material characteristics derived from the actual acquisition instead of a separate calibration scan. A superior method would be to perform a scan with the basis materials included to use as calibration for the image acquisition of the scanned object. This method would remove the manual component of the decomposition process, so any differences between decompositions would be completely due to changes in the image acquisition or decomposition parameters, not the user. In this work, we have not considered or tested when the materials mix. Theoretically, the decomposed intensity should scale with the makeup of the mixing. If a mixture of materials is 50% of one and 50% of the other, the decomposed maps should have 50% of maximum intensity in both of the maps, depending on the density of the materials in the final mixture.

An important consideration for the eventual application of material decomposition is the added dose that is delivered to the scanned object because of the dual-energy CT acquisition. Two CT scans are currently required, nearly doubling the dose delivered to the patient in a clinical setting. Future solutions to this problem may involve the use of single photon counting detectors capable of acquiring spectral CT image data in a single CT scanning process, thereby preventing the need for a second CT scan. This means that a dual-energy CT scan could take place without any increase in dose to the patient, depending on the statistics required. Such detectors with high resolution for use in CBCT are currently under development and hold great promise for the future. Nevertheless, the current risk vs. benefit assessment for this sort of dual-energy scanning will have to be considered for clinical application.

There are multiple methods that researchers have developed to obtain patient DE spectral CT data, keeping in mind that two separate scans such as what was carried out during this work would not provide enough image registration between the two scans due to patient motion. Siemens developed a system that employs two tubes operating at a different voltage, and two separate detector panels[16]. The tubes are offset spatially from each other by some angle, offset by some energy from each other, and complete a sweep of the patient at the same time. General Electric has a system that uses one tube with rapid kVp switching, and one detector panel[17]. Philips has a system that uses one tube with a single tube voltage, and a stack of two detector panels[18]. The front panel attenuates the low energy photons; the back panel attenuates the high-energy photons. The method used to obtain the data in this work was less complicated in that separate complete acquisitions are carried out for each beam energy. Due to the use of higher resolution detectors; however, this approach may be more applicable to higher resolution cone-beam CT applications.

5. CONCLUSIONS

This project was involved with the investigation of the application of material decomposition specifically applied on images acquired of the neurovasculature to plan, carry out, and assess image-guided interventions. The use of dual-energy CT in this application utilizes the variation in attenuation coefficient of materials as the energy changes, and is able to obtain image data with better differentiation of the devices and contrast agents often used in this application.

This specific work utilized both a 3D-printed simple aneurysm model imaged using a micro-CT system coupled to a CMOS detector, as well as an angiographic head phantom imaged using a c-arm CBCT system. Our preliminary results indicate the potential to utilize high-resolution scan data to identify stent struts and individual coil loops, even when they are in close proximity to contrast agent. This creates a situation where single-energy CT would not be able to obtain images with as much material separation between the devices, contrast, and actual vasculature. This was confirmed through the use of qualitative assessment, as well as the computation of the %NRMSE metric, which compares the result of the decomposition with the expectation of the result.

These results indicate the potential for clinical utility, dependent on results of further testing and validations. Moving forward, we will look to investigate new quantitative metrics to better assess and optimize the decomposition process, as well as other types of endovascular procedures such as the deployment of high-Z embolization agents for the treatment of arteriovenous malformations. It may also prove useful to perform this sort of testing considering phantoms with anatomy that is more complex, as well as containing overlapping structure.

Acknowledgments

This work is supported by NIH grant 2R01EB002873 and by an equipment grant from Toshiba Medical Systems Corporation.

References

1. Wang X, Meier D, Taguchi K, Wagenaar DJ, Patt BE, Frey EC. Material separation in x-ray CT with energy resolved photon-counting detectors. Med Phys. Mar; 2011 38(3):1534–46. [PubMed: 21520865]
2. Kroft LJ, deRoos A, Geleijns J. Review. Artifacts in ECG-Synchronized MDCT Coronary Angiography. Am J Roentgenol. 2007; 189(3)
3. Graser A, Johnson RC, Chandarana H, Macari M. Dual energy CT: preliminary observations and potential clinical applications in the abdomen. Eur Radiol. Jan.2009 19(13)
4. Hubbell JH, Seltzer SM. Tables of X-Ray Mass Attenuation Coefficients and Mass Energy-Absorption Coefficients from 1 keV to 20 MeV for Elements Z = 1 to 92 and 48 Additional Substances of Dosimetric Interest, NIST Standard Reference Database. 1996:126.
5. Yu L, Leng S, McCollough CH. Dual-energy CT-based monochromatic imaging. Amer J Roentgenology. Nov.2012 199(5 supplement)
6. Johnson TRC, et al. Material Differentiation by Dual Energy CT: Initial Experience. Eur Radiol. 2007; 17(6):1510–1517. [PubMed: 17151859]
7. Shikhaliev PM. Photon counting spectral CT: improved material decomposition with Kedge-filtered x-rays. Phys Med Biol. 2012; 57(6)
8. Wu HW, et al. Pulmonary embolism detection and characterization through quantitative iodine-based material decomposition images with spectral computed tomography imaging. Invest Radiol. 2012; 47(1):85–91. [PubMed: 22107805]
9. Mendonca PRS, et al. Initial evaluation of virtual un-enhanced imaging derived from fast kVp-switching dual energy contrast enhanced CT for the abdomen. Proc SPIE 7622. 2011
10. Friedman SN, et al. Computed tomography (CT) bone segmentation of an ancient Egyptian mummy: a comparison of automated and semiautomated threshold and dual-energy techniques. J Comput Assist Tomogr. 2012; 36(5):616–622. [PubMed: 22992615]
11. Ionita CN, Hoffmann KR, Bednarek DR, Chityala R, Rudin S. Cone-beam micro-CT system based on LabVIEW software. J Digit Imaging. Sep; 2008 21(3):296–305. [PubMed: 17333411]
12. Feldkamp LA, et al. Practical cone-beam algorithm. J Opt Soc Am. 1984; 1(6):612–619.
13. Patel V, Chityala RN, Hoffman KR, Ionita CN, Bednarek DR, Rudin S. Self-calibration of a cone-beam micro-CT system. Med Phys. Jan; 2009 36(1):48–58. [PubMed: 19235373]
14. Lee S, et al. Quantitative material decomposition using spectral computed tomography with an energy-resolved photon-counting detector. Phys Med Biol. 2014; 59(18):5457–5482. [PubMed: 25164993]
15. Podgorsak, AR., Nagesh, SVS., Bednarek, DR., Rudin, S., Ionita, CN. Implementation of material decomposition using an EMCCD and CMOS-based micro-CT system. Proc. SPIE 10137, Medical Imaging 2017: Biomedical Applications in Molecular, Structural, and Functional Imaging, 1013714; March 13, 2017;
16. Flohr TG, et al. First performance evaluation of a dual-source CT (DSCT) system. Eur Radiol. 2006; 16(2):256–268. [PubMed: 16341833]
17. Eusemann C, et al. Dual energy CT: How to best blend both energies in one fused image? Proc SPIE 6918. 2008
18. Carni, R., et al. Material separation with dual-layer CT. IEEE Sci. Symp Conf Record; 2005;

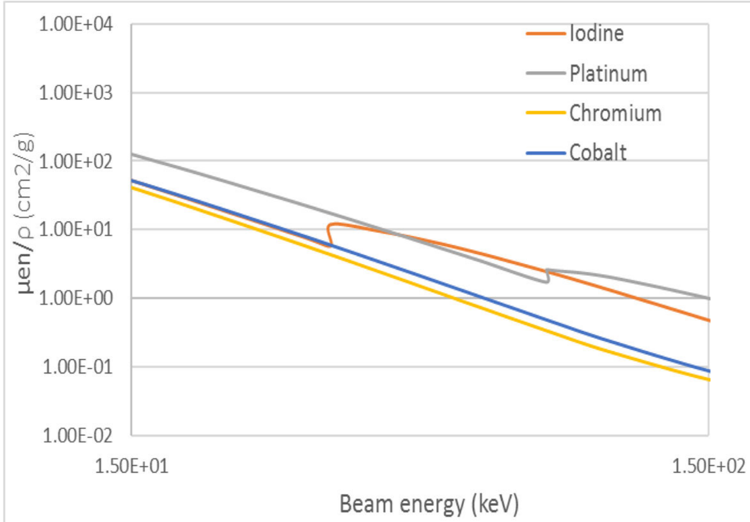

Figure 1.

Plot detailing how the attenuation coefficient of selected materials specific to the context of neurovascular intervention varies with changing energy in the range of diagnostic radiography. Note the similarity of the materials, leading to difficulty in separation with single energy CT. Data from NIST[4].

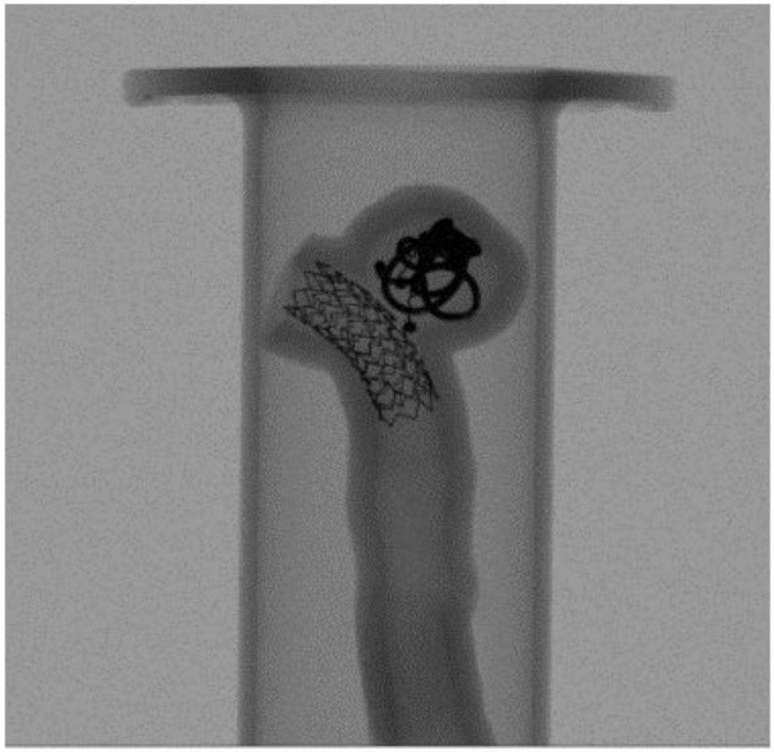

Figure 2.
Projection image of simple aneurysm model. Visible is the platinum coil deployed into the aneurysm orifice, and cobalt-chromium stent which spans the orifice.

Author Manuscript
Author Manuscript
Author Manuscript

Figure 3.
Image of RS-240T angiographic head phantom containing vascular insert filled with iodine.

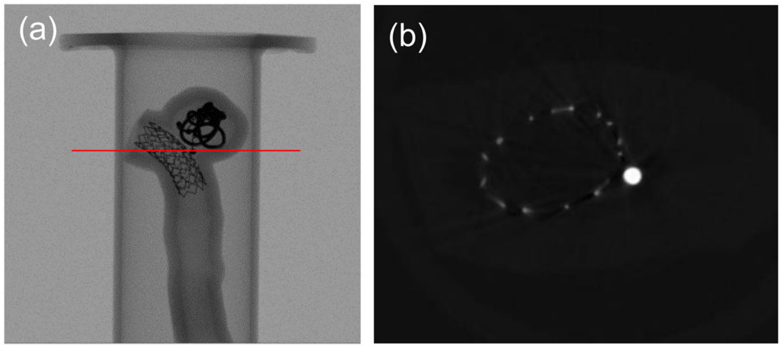

Figure 4.

(a) shows a projection image of the simple aneurysm model prior to the addition of iodine contrast agent. Included on the figure is a red plane marking where reconstruction occurred to obtain the image on the right. (b) is a reconstructed slice of the model using the projection data shown on the left. Visible in both images are the platinum coil and the cobalt-chromium stent.

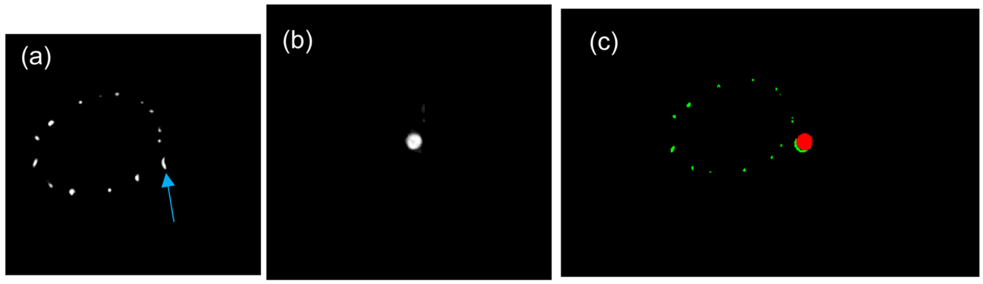

Figure 5.

(a) shows the cobalt-chromium contribution to the reconstructed slice shown in Fig. 4b. Blue arrow details a region of error in the decomposed space. (b) shows the contribution of platinum to the reconstructed slice. (c) is the two slices recolored and overlaid on each other. Red is the platinum, green is the cobalt-chromium.

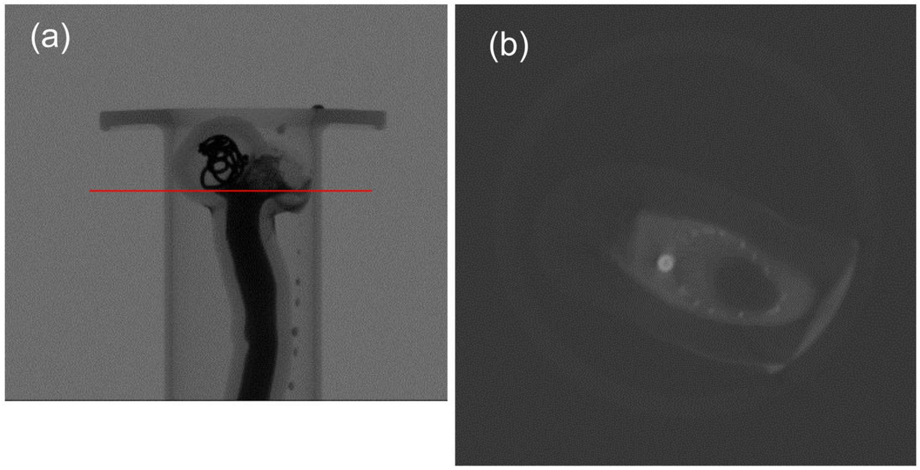

Figure 6.

(a) shows a projection image of the simple aneurysm model following the addition of the iodine contrast agent. Recall that this model simulates a case following thrombosis of the aneurysm, so no contrast is expected to fill the aneurysm sac. Included on the figure is a red plane marking where reconstruction occurred to obtain the image on the right. (b) is a reconstructed slice of the model using the projection data shown on the left. Visible in both images are the iodine contrast agent, the cobalt-chromium stent, and the platinum coil.

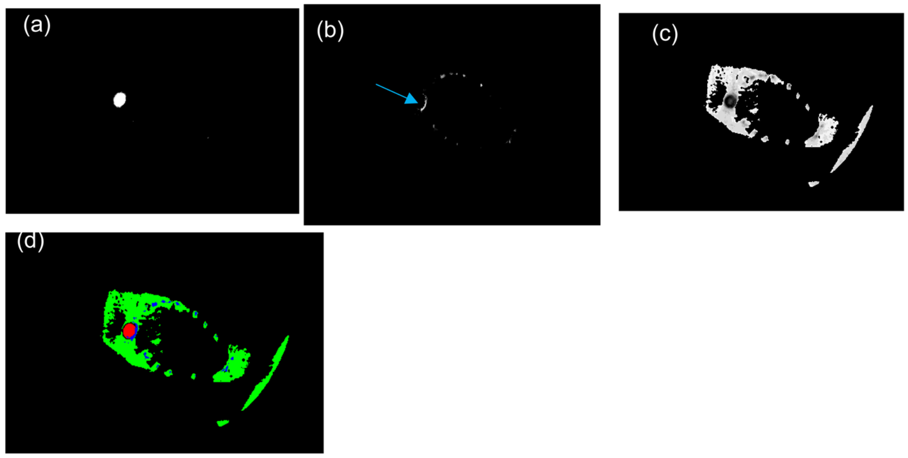

Figure 7.

(a) shows the platinum contribution to the reconstructed slice shown in Fig. 6b. (b) shows the cobalt chromium contribution to the reconstructed slice. Included is a blue arrow showing evidence of error in the decomposed space. (c) shows the iodine contribution to the reconstructed slice. (d) is the three slices recolored and overlaid onto each other. Red is platinum, blue is cobalt-chromium, green is iodine.

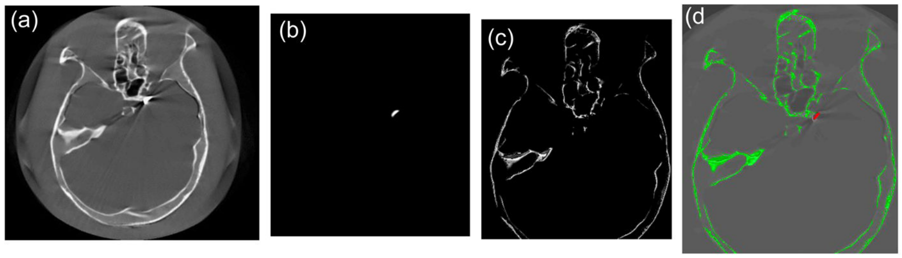

Figure 8.

(a) is an example slice used for material decomposition between iodine and bone in the RS-240T angiographic head phantom. (b) is the slice decomposed into iodine. (c) is the slice decomposed into the bone. (d) is the result of the decomposition overlaid into the original slice with color. Red is the iodine insert, green is the bone of the skull insert. Note the ability of the decomposition process to use anatomical information collected from a flat panel detector.

Figure 9.
Maximum intensity projection of RS-240T angiographic phantom showing a different way the result of decomposition may be displayed. The green is the pure cortical bone and the orange is the iodine insert. Error at the superior end of the phantom may be due to misalignment of the rotational axis of scanned object with CBCT system. Note the good agreement of the decomposition with the input image data.

Table 1

Results of percent NRMSE computation for the decomposition between cobalt-chromium and platinum. Both basis materials were decomposed with superior to the 10% NRMSE threshold. Due to the error present in the cobalt-chromium map, the % NRMSE is higher than that of the platinum.

NRMSE (%)	
Co-Cr	5.81
Platinum	0.32

Author Manuscript

Author Manuscript

Author Manuscript

Table 2

Results of %NRMSE computation for the decomposition between cobalt-chromium, platinum, and iodine. All three of the materials were decomposed so that the %NRMSE is below the 10% threshold. The cobalt-chromium was the least accurate decomposition due to the shape of the struts being impacted by the reconstruction artifacts, as well as the error present in the CoCr mapping of the decomposition. The addition of the iodine reduced the accuracy of the platinum and CoCr decomposition.

NRMSE (%)	
Co-Cr	8.9
Platinum	1.04
Iodine	3.6